



Since January 2020 Elsevier has created a COVID-19 resource centre with free information in English and Mandarin on the novel coronavirus COVID-19. The COVID-19 resource centre is hosted on Elsevier Connect, the company's public news and information website.

Elsevier hereby grants permission to make all its COVID-19-related research that is available on the COVID-19 resource centre - including this research content - immediately available in PubMed Central and other publicly funded repositories, such as the WHO COVID database with rights for unrestricted research re-use and analyses in any form or by any means with acknowledgement of the original source. These permissions are granted for free by Elsevier for as long as the COVID-19 resource centre remains active.



Porcine epidemic diarrhea virus papain-like protease 2 can be noncompetitively inhibited by 6-thioguanine

Hsu-Feng Chu^{a,b}, Chiao-Che Chen^b, David C. Moses^c, Yau-Hung Chen^c, Chao-Hsiung Lin^b, Ying-Chieh Tsai^{d,e}, Chi-Yuan Chou^{b,*}

^a Biomedical Industry Ph.D. Program, National Yang-Ming University, Taipei 112, Taiwan

^b Department of Life Sciences and Institute of Genome Sciences, National Yang-Ming University, Taipei 112, Taiwan

^c Department of Chemistry, Tamkang University, Tamsui 251, Taiwan

^d Institute of Biochemistry and Molecular Biology, National Yang-Ming University, Taipei 112, Taiwan

^e Probiotic Research Center, National Yang-Ming University, Taipei 112, Taiwan



ARTICLE INFO

Keywords:

PEDV
Papain-like protease
6-Thioguanine
Noncompetitive inhibition
Alpha coronavirus

ABSTRACT

Porcine epidemic diarrhea virus (PEDV) is a coronavirus (CoV) discovered in the 1970s that infects the intestinal tract of pigs, resulting in diarrhea and vomiting. It can cause extreme dehydration and death in neonatal piglets. In Asia, modified live attenuated vaccines have been used to control PEDV infection in recent years. However, a new strain of PEDV that belongs to genogroup 2a appeared in the USA in 2013 and then quickly spread to Canada and Mexico as well as Asian and European countries. Due to the less effective protective immunity provided by the vaccines against this new strain, it has caused considerable agricultural and economic loss worldwide. The emergence of this new strain increases the importance of understanding PEDV as well as strategies for inhibiting it. Coronaviral proteases, including main proteases and papain-like proteases, are ideal antiviral targets because of their essential roles in viral maturation. Here we provide a first description of the expression, purification and structural characteristics of recombinant PEDV papain-like protease 2, moreover present our finding that 6-thioguanine, a chemotherapeutic drug, in contrast to its competitive inhibition on SARS- and MERS-CoV papain-like proteases, is a noncompetitive inhibitor of PEDV papain-like protease 2.

1. Introduction

Discovered in the 1970s, porcine epidemic diarrhea virus (PEDV) is a coronavirus that causes severe agricultural loss (Chasey and Cartwright, 1978; Lee, 2015). PEDV infects the intestinal tract and causes diarrhea and vomiting in older pigs. The mortality of PEDV-infected piglets can reach 100% due to extreme dehydration (Stevenson et al., 2013). Recently, modified live attenuated vaccines for PEDV genogroup 1 has been an important way to control the spreading of PEDV in Asia (Song and Park, 2012). In 2013, a new vaccine-resistant PEDV strain, appeared in the USA (Stevenson et al., 2013). Since then, this new USA PEDV strain, which was later assigned to genogroup 2a, has caused a continuous pandemic in North America, Europe and Asia (Huang et al., 2013; Song et al., 2015). The resistance of the new PEDV

strain to the conventional vaccine highlights the issue that although vaccination is a powerful strategy, it can still fail due to the genetic diversity of epitopes between genogroups. As a result, it is necessary to develop another antiviral strategy for PEDV.

Unlike two other highly pathogenic human CoVs, severe acute respiratory syndrome coronavirus (SARS-CoV) and Middle East respiratory syndrome coronavirus (MERS-CoV), which belong to the beta group, PEDV belongs to the alpha group (Chan et al., 2015). Like other CoVs, PEDV depends on its own proteases, including main protease (M^{Pro}) and papain-like protease (PL^{Pro}) to cleave the polyprotein, and alpha CoVs have both papain-like protease 1 (PL1^{Pro}) and papain-like protease 2 (PL2^{Pro}) (Lee, 2015; Wojdyla et al., 2010). Polyprotein cleavage is required for viral maturation and thus these proteases are ideal antiviral targets (Bacha et al., 2008; Cheng et al., 2015; Chou

Abbreviations: AUC, The abbreviations used are analytical ultracentrifugation; CoV, coronavirus; DUB, deubiquitinating; MERS, Middle East respiratory syndrome; β ME, β -mercaptoethanol; 6MP, 6-mercaptapurine; nsp, non-structural protein; PL^{Pro}, papain-like protease; PL1^{Pro}, papain-like protease 1; PL2^{Pro}, papain-like protease 2; PEDV, porcine epidemic diarrhea virus; 6TG, 6-thioguanine; SARS, severe acute respiratory syndrome; SV, sedimentation velocity; Ubl, ubiquitin-like; Ub-AFC, ubiquitin-7-amino-4-trifluoro-methyl-coumarin; USP, ubiquitin-specific protease

* Corresponding author. 155 Li-Nong St., Sec. 2, Taipei 112, Taiwan.

E-mail address: cychou@ym.edu.tw (C.-Y. Chou).

<https://doi.org/10.1016/j.antiviral.2018.08.011>

Received 18 April 2018; Received in revised form 9 July 2018; Accepted 17 August 2018

Available online 20 August 2018

0166-3542/ © 2018 Elsevier B.V. All rights reserved.

et al., 2008; Kumar et al., 2017; Lin et al., 2018; Park et al., 2012; Ratia et al., 2008; Wu et al., 2006). Furthermore, in contrast to highly variable spike proteins targeted by antibodies (Li et al., 2005, 2017; Wang et al., 2013; Wu et al., 2009), proteases with more conserved structure and catalytic function may serve as a general target across different CoVs (Anand et al., 2003; Bailey-Elkin et al., 2014; Chou et al., 2014; Ho et al., 2015; Ratia et al., 2006; Yang et al., 2003).

Like other coronaviral PL^{pro}s, PEDV PL2^{pro} is not only a deubiquitinating (DUB) protease but also a multifunctional protein which plays a role in regulating host antiviral immune response (Chaudhuri et al., 2011; Clementz et al., 2010; Mielech et al., 2014; Xing et al., 2013; Zheng et al., 2008). DUB activity of PL2^{pro} is required for the suppression of host immunity by blocking type 1 interferon signaling. However, up to now, the structural characteristics and the detailed catalytic mechanism of PEDV PL2^{pro} are still unclear, as are strategies for its inhibition.

According to sequence alignment (Fig. S1) and homology modeling, PEDV PL2^{pro} may be composed of four domains: ubiquitin-like (Ubl), palm, thumb and fingers domains. The latter three domains form a catalytic core and may retain catalytic activity, like that of SARS- and MERS-CoV PL^{pro}s (Chou et al., 2012; Clasman et al., 2017; Lei et al., 2014). In the present study, we made a recombinant catalytic core PEDV PL2^{pro} and demonstrated its secondary, tertiary and quaternary structural characteristics. Further studies suggest that PEDV PL2^{pro} exhibits much higher DUB activity than that of SARS- and MERS-CoV PL^{pro}s and can be inhibited by the anti-leukemia drug 6-thioguanine (6TG). 6TG has been found to be able to inhibit multiple DUB enzymes including human USP2 as well as SARS- and MERS-CoV PL^{pro}s (Chen et al., 2009; Cheng et al., 2015; Chou et al., 2008; Chuang et al., 2018; Lin et al., 2018). Inhibition assays and docking simulations were used to clarify the detailed inhibition mechanism of 6TG against PEDV PL2^{pro}. Our findings increase understanding of the structure and catalytic activity of PEDV PL2^{pro} and identify the first potent inhibitor against this enzyme.

2. Materials and methods

2.1. Construction of expression plasmids

The coding sequence of the USA strain of PEDV PL2^{pro} Ubl and catalytic domain (GenBank accession number [AHC03501.1](#); poly-protein residues 1630–1922) was full-gene synthesized (Genomics Co., Taiwan). cDNA of PL2^{pro} digested by *NdeI* and *XhoI* was then inserted into pET-28a and pET-29a expression vectors, respectively. For the catalytic core of PL2^{pro} (residues 1686–1922), the primers 5'-GGCTCC GCGAATTGGGATTC-3' and 5'-AAAACGAGTCATTCGACACCAC CACATTG-3' were used for polymerase chain reaction. The product was digested with *XhoI* and then ligated into a pHD vector with a 6× His-tag and a SUMO (SMT3) sequence at the N-terminus (Lee et al., 2008). The primer sequences for site-directed mutagenesis of the T39W mutant were 5'-GAATGGCCGTCGTGTGCTGAAATGGACCGATAATAATTGC TGG-3' and 5'-CCAGCAATTATTATCGGTCCATTCAGCACACGACGGC CATT-3'. The reading frames of the above plasmids were verified by DNA sequencing.

2.2. Recombinant PEDV PL2^{pro} production

The expression vector was transformed into *E. coli* BL21 (DE3) cells (Novagen). Cultures were grown in LB medium at 37 °C until the absorbance at 600 nm reached 0.6. The cells were then induced with 1 mM isopropyl-β-D-thiogalactopyranoside and incubated for 20 h at 20 °C. After centrifugation, the cell pellet was suspended in lysis buffer (20 mM Tris-Cl, pH 8.5, 250 mM NaCl, 5% glycerol, 0.2% Triton X-100 and 2 mM β-mercaptoethanol) and lysed by sonication. Next, the crude lysate was centrifuged at 12,000 rpm for 20 min. The soluble lysate was incubated with 2 ml of Ni-NTA agarose slurry (Qiagen Co., USA) at 4 °C

for 1 h. After the unbound lysate removed, the beads were washed with wash buffer (20 mM Tris-Cl, pH 8.5, 250 mM NaCl, 8 mM imidazole and 2 mM β-mercaptoethanol). The beads with 6× His-tag protein bound were then transferred into 3.5 ml cutting buffer (20 mM Tris-Cl, pH 8.5, 250 mM NaCl, and 2 mM β-mercaptoethanol), 0.1 mg Ulp1 was added, and the mixture was incubated at 25 °C for 4 h to remove the SUMO fusion. Finally, unbound PEDV PL2^{pro} catalytic core was loaded onto an S-100 gel-filtration column (GE Healthcare) equilibrated with running buffer (20 mM Tris-Cl, pH 8.5, 100 mM NaCl and 2 mM dithiothreitol). Each protein fraction was checked for purity using SDS-PAGE. Fractions containing a protein band of the correct size were then pooled and concentrated using an Amicon Ultra-4 10-kDa filter (Millipore) to 20 mg/ml. The protein with 5% glycerol was flash-frozen with liquid nitrogen and stored at –80 °C. The typical yield of protein was 3–5 mg per liter of cell culture.

2.3. Circular dichroism (CD) spectroscopy

A JASCO J-810 spectropolarimeter was used to analyze the secondary structure. Recombinant PEDV PL2^{pro} at a concentration of 1 mg/ml in 20 mM phosphate buffer (pH 6.5) was used for CD scanning from 250 nm to 190 nm at 20 °C. The cuvette width was 0.1 mm. The far-UV CD spectrum data was analyzed using the CDSSTR program at the DichroWeb server (Whitmore and Wallace, 2008). The normalized root mean square deviation was calculated to evaluate goodness of fit.

2.4. Spectrofluorimetric analysis

The fluorescence spectrum of 0.5 μM protein dissolved in 20 mM phosphate buffer (pH 6.5) or 5.4 M guanidine hydrochloride was monitored at 25 °C using a PerkinElmer LS50B luminescence spectrometer. The excitation wavelength was 280 nm and the emission spectrum was scanned from 300 nm to 400 nm. Measurements of maximal peak and intensity were used to identify conformational change.

2.5. Analytical ultracentrifugation analysis (AUC)

AUC experiments were performed on an XL-A analytical ultracentrifuge (Beckman Coulter) using an An-60 Ti rotor. Sedimentation velocity (SV) experiments were performed using a double-sector epon charcoal-filled centerpiece at 20 °C at a rotor speed of 42,000 rpm. A protein solution of 0.4 mg/ml PEDV PL2^{pro} catalytic core and reference solutions (20 mM Tris-Cl, pH 8.5, 100 mM NaCl) were loaded into the centerpiece. Absorbance at 280 nm was monitored continuously with a time interval of 500 s and a step size of 0.003 cm. Multiple scans at different time intervals were fitted to a continuous c(s) and c(M) distribution model using the SEDFIT program (Schuck, 2000).

2.6. DUB assay

For DUB assays, the reaction mixtures contained 0.25 μM of fluorogenic substrate ubiquitin-7-amino-4-trifluoro-methyl-coumarin (Ub-AFC) (Boston Biochem) and 0.17 μM of SARS- or MERS-CoV PL^{pro} or 0.004 μM of PEDV PL2^{pro} in 20 mM phosphate buffer (pH 6.5) for a total volume of 0.5 ml. Enzymatic activity at 30 °C was determined by monitoring excitation and emission at 350 and 485 nm, respectively. To determine the inhibitory effect, velocity data at various concentrations of inhibitors was fitted to obtain IC₅₀ according to Eq. (1):

$$v = v_0 / (1 + IC_{50}^n / [I]^n) \quad (1)$$

in which v is the initial velocity in the presence of inhibitor at concentration $[I]$ and v_0 is the initial velocity in the absence of inhibitor, while n is the Hill constant. The program SigmaPlot 12.5 (Systat Software) was used for data analysis.

2.7. Steady-state kinetic analysis

The peptidyl substrates Dabcyl-FRLKGGAPIKGV-Edans and Dabcyl-FKKKGGDVKE-Edans (synthesized by GenScript) were used to measure the proteolytic activity of the PEDV PL2^{pro} catalytic core and the T39W mutant. Increases in fluorescence intensity were monitored at excitation and emission wavelengths of 329 and 520 nm, respectively, in a PerkinElmer LS50B luminescence spectrometer. Fluorescence intensity was converted to the concentration of hydrolyzed substrate using a standard curve determined by fluorescence measurements of defined concentrations of products. For kinetic analysis, the reaction mixtures contained 5–50 μM peptide substrate in 20 mM phosphate buffer (pH 6.5) for a total volume of 1 ml. After the addition of enzyme to the reaction mixture to a concentration of 3.85 μM , the fluorescence intensity was monitored at 30 °C. The increase in fluorescence intensity was linear for 3 min and thus the slope of the line represented the initial velocity. Steady-state kinetic parameters were determined by fitting the data to the Michaelis-Menten equation.

2.8. Determination of inhibition mechanism

Enzyme kinetic assays were performed by a method similar to that described above at peptidyl substrate concentrations of 10–50 μM and inhibitor concentrations of 0–60 μM . The velocity data was found to best fit a noncompetitive inhibition model in accordance with Eq. (2):

$$v = k_{\text{cat}} [E][S] / ((1 + [I]/K_{\text{is}})(K_{\text{M}} + [S])) \quad (2)$$

in which k_{cat} is the rate constant, $[E]$, $[S]$ and $[I]$ denote the enzyme, substrate and inhibitor concentrations, respectively, and K_{M} is the Michaelis constant for the interaction between the peptide substrate and the enzyme. K_{is} is the inhibition constant.

2.9. Structure modeling and docking simulation

The model structure of PEDV PL2^{pro} was generated by SWISS-modeling (Arnold et al., 2006) and molecular docking was performed using AutoDock Vina (Trott and Olson, 2010). Several grid boxes of 27000 \AA^3 (30 $\text{\AA} \times 30 \text{\AA} \times 30 \text{\AA}$) with different centering coordinates were set to cover the entire putative structure. The docking parameters were set as default and the best 10 models in each coordinate set were listed for further inspection. The model that scored the best among these sets was selected as the final binding model.

3. Results and discussion

3.1. Production of recombinant PEDV PL2^{pro}

Initially, attempts at expressing PEDV PL2^{pro} including the Ubl and catalytic domains (polyprotein residues 1630–1922) with either an N-terminal or a C-terminal 6 \times His-tag were not successful. Previous studies suggested that the Ubl domain was not involved in the catalytic activity of SARS- and MERS-CoV PL^{pro}s (Chou et al., 2012; Clasman et al., 2017). Therefore we removed the Ubl domain and applied a SUMO fusion protein at the N-terminus of the catalytic core (residues 1686–1922) to enhance solubility. Fortunately, it was possible to express the PEDV PL2^{pro} catalytic core in *E. coli* and purify it following the removal of SUMO. After further purification using size-exclusion chromatography, highly pure PL2^{pro} was obtained (Fig. S2, left panel, lane 6). Mass spectrometry was performed to identify the sequence of the recombinant protein. In total, 19 peptides originating from PEDV PL2^{pro} were identified (Fig. S2, right panel). Alignment of these peptides with the PEDV PL2^{pro} sequence shows 60% coverage, and both the N-terminus and C-terminus of the protein were confirmed (Fig. S2, bottom panel).

3.2. Secondary, tertiary and quaternary structural analysis

As this is the first time that pure PEDV PL2^{pro} has been obtained, its secondary, tertiary and quaternary structures were further analyzed. CD spectrometry and analysis of the spectrum by CDSSTR (Fig. S3A) showed that PEDV PL2^{pro} consists of 27% α -helix, 29% β -sheet and 44% random coil. These proportions are similar to those of the SARS-CoV PL^{pro} core (residues 1600–1858), which consists of 21% α -helix, 29% β -sheet and 49% random coil (data not shown). For comparison, previous studies suggested that MERS-CoV PL^{pro} consists of 23% α -helix, 36% β -sheet and 38% random coil, where the higher content of β -sheet is because of the inclusion of the Ubl domain (Lin et al., 2014). Our results suggest that the three coronaviral PL^{pro}s show similar secondary structural content.

Protein emission was used to reveal tertiary conformational change in the absence and presence of denaturant (Fig. S3B). The results demonstrated that the fluorescence emission of PEDV PL2^{pro} in phosphate buffer (native form) shows a major broad peak at 330 nm which splits to two peaks at 310 nm and 360 nm in 5.4 M guanidine hydrochloride. The two peaks match the maximal emission wavelengths of tyrosine and tryptophan, respectively. This result suggests that the addition of denaturant induces exposure of the hydrophobic core of the protein. Similar folding/unfolding change at maximal emission wavelength was also observed in the case of SARS-CoV PL^{pro}, albeit the fluorescence intensity of denatured PEDV PL2^{pro} is higher than that of the native enzyme (Chou et al., 2012). Previous studies on the stability of the P53 core domain suggested that the higher fluorescence intensity of denatured P53 is because of aggregation (Bullock et al., 1997).

SV experiments were carried out to determine the quaternary structure of PEDV PL2^{pro} (Fig. S4A). Using continuous c(s) and c(M) distribution analysis, we found one major peak with a sedimentation coefficient of 2.4 and molecular weight of 25 kDa (Figs. S4B and S4C). This value is close to the predicted monomeric mass (25.8 kDa). Previous studies using the same SV experiment suggested that both the SARS- and MERS-CoV PL^{pro}s are also monomers (Chou et al., 2014; Lin et al., 2014). Overall, the secondary, tertiary and quaternary structures of the PEDV PL2^{pro} catalytic core are similar to those of SARS- and MERS-CoV PL^{pro}s, even though their sequence identity is only 22–25% (Fig. S1).

3.3. DUB and proteolytic activity of PEDV PL2^{pro}

Next, in order to compare the DUB activity of PEDV PL2^{pro} with other coronaviral PL^{pro}s, activity assays using Ub-AFC as the substrate were carried out. The activity was determined and then normalized to give the fold increase in DUB activity of PEDV PL2^{pro} (Fig. 1). The results showed that SARS- and MERS-CoV PL^{pro}s have similar DUB activity. Surprisingly, at a given substrate concentration, PEDV PL2^{pro} shows activity comparable to that of the other two PL^{pro}s at only one-fourth of the protein concentration. This indicates that PEDV PL2^{pro} has considerably greater DUB activity. Furthermore, sequence alignment indicates that PEDV PL2^{pro} may also have a zinc fingers motif like other coronaviral PL^{pro}s (Fig. S1, green ovals) (Bailey-Elkin et al., 2014; Lei et al., 2014; Ratia et al., 2006; Wojdyla et al., 2010). Previous studies have shown that the DUB activity of coronaviral PL^{pro}s can be inhibited by the addition of a chelator like EDTA, which removes intrinsic zinc ions (Chou et al., 2008; Lin et al., 2014). In line with our expectations, inhibition of PEDV PL2^{pro} by EDTA displays a similar dose-dependent pattern, suggesting that the removal of endogenous metal ions can inhibit PEDV PL2^{pro} (Fig. 1). Furthermore, like other coronaviral PL^{pro}s, PEDV PL2^{pro} can be inhibited by adding extra external zinc ions (Chou et al., 2008; Lin et al., 2014).

In addition, the proteolytic activity of PEDV PL2^{pro} was investigated using fluorogenic peptidyl substrates (Table 1). For comparison, we used a peptidyl substrate with a sequence matching the P6 to P1 residues of the cleavage site of SARS-CoV PL^{pro}, FRLKGG, and a peptidyl

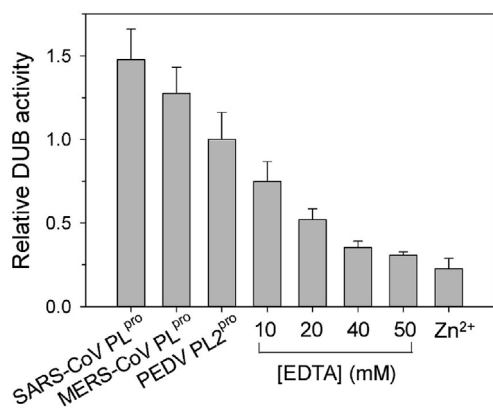


Fig. 1. DUB activity analysis of coronaviral PL^{pro} and PL2^{pro}. (A) Relative DUB activities of MERS-CoV PL^{pro} (0.17 μ M), SARS-CoV PL^{pro} (0.17 μ M) and PEDV PL2^{pro} (0.004 μ M). Inhibition of PEDV PL2^{pro} by 10–50 mM EDTA or 50 μ M Zn²⁺ were also measured. Activity data of each set was normalized to that of PEDV PL2^{pro}.

substrate optimized for PEDV PL2^{pro} whose cleavage site P6 to P1 residues are FKKKGG, based on the non-structural protein (nsp) 2 to 3 cleavage site (from GenBank accession number [AHC03501.1](#)). Interestingly, less saturation was observed while using the optimized peptidyl substrate (Fig. S5A). We failed to improve it due to the fact that the proteolytic activity at concentrations of substrate higher than 50 μ M cannot be appropriately measured because of the inner-filter effect. After fitting the data to the Michaelis-Menten equation, K_m of 18.6 μ M and k_{cat} of 0.065 min^{-1} for the SARS-CoV-derived substrate and the K_m of 61.6 μ M and k_{cat} of 0.299 min^{-1} for the optimized substrate were determined (Table 1). The optimized substrate shows a 1.4-fold higher k_{cat}/K_m , as a result of a 3.3-fold higher K_m and 4.6-fold higher k_{cat} , compared with the SARS-CoV-derived substrate. The dissimilar kinetic parameters for the two peptidyl substrates suggest that PEDV PL2^{pro} may recognize various P4 residues between beta CoVs (L/F/V/G) and alpha CoVs (K/R/A). By contrast, SARS-CoV PL^{pro} has a hydrophobic S4 subsite, with the result that it cannot cleave the PEDV-optimized substrate and substrates of HCoV-229E and IBV whose P4 residue is also a lysine (Chou et al., 2014; Han et al., 2005; Lei et al., 2018; Wojdyla et al., 2010). Furthermore, in contrast to its considerably greater DUB activity, k_{cat} of PEDV PL2^{pro} for the optimized peptidyl substrate is 22-fold lower than that of SARS-CoV PL^{pro} (Lin et al., 2014). The inconsistent efficacy between DUB and proteolytic activities indicates that PEDV PL2^{pro} is more like a USP enzyme (Avvakumov et al., 2006; Renatus et al., 2006). Previous studies have suggested that PEDV PL2^{pro}, but not PL1^{pro}, is an interferon antagonist via its DUB activity (Xing et al., 2013). In addition, a recent review suggests that PL1^{pro} and PL2^{pro} of alpha CoVs may show different levels of efficiency for cleaving the nsp 1 to 2, 2 to 3 and 3 to 4 sites (Lei et al., 2018).

Previous studies of SARS-CoV PL^{pro} demonstrated that the oxyanion is within hydrogen-bonding distance of the side chain of Trp107 during catalysis (Ratia et al., 2006). Although it is not conserved, mutation of the equivalent residue Leu105 of MERS-CoV PL^{pro} to tryptophan showed a 41-fold increase in k_{cat} (Lin et al., 2014). Again, according to

Table 1

Steady-state apparent kinetic parameters of PEDV PL2^{pro} and its T39W mutant.

Peptidyl substrate	PEDV PL2 ^{pro}	K_m (μ M)	k_{cat} (min^{-1})	k_{cat}/K_m ($\mu\text{M}^{-1}\text{min}^{-1}$)
Dabcyl-FRLKGGAPIKGV-Edans	Wild-type	18.6 \pm 4.3	0.065 \pm 0.006	0.0035
	T39W	32.1 \pm 12	1.050 \pm 0.198	0.0327
Dabcyl-FKKKGGGDVKE-Edans	Wild-type	61.6 \pm 19.7	0.299 \pm 0.061	0.0049
	T39W	39.6 \pm 15.6	0.247 \pm 0.053	0.0062

The steady-state apparent kinetic data for hydrolyzing either Dabcyl-FRLKGGAPIKGV-Edans (SARS-CoV-derived) or Dabcyl-FKKKGGGDVKE-Edans (PEDV-derived) substrates were determined according to the Michaelis-Menten equation. R_{sq} were 0.964, 0.938, 0.976, and 0.944.

sequence alignment, the equivalent residue of PEDV PL2^{pro} is Thr39 (Fig. S1, purple oval). To verify this, a T39W mutant was produced and its kinetic parameters were characterized by using the two peptidyl substrates (Fig. S5B and Table 1). Interestingly, using the SARS-CoV-derived substrate produced a 9.3-fold increase in activity based on k_{cat}/K_m as a result of a 1.7-fold increase in K_m and a 16-fold increase in k_{cat} . This result demonstrates that the mutation enhances hydrolysis of the SARS-CoV-derived peptidyl substrate. In contrast, there is no significant difference in hydrolysis of the optimized substrate between wild-type PEDV PL2^{pro} and the T39W mutant (Table 1). This result indicates that the existence of residue Thr39 may be quite enough to support proteolytic ability. Further structural information on PEDV PL2^{pro} in complex with Ub or the optimized peptidyl substrate is required to demonstrate the detailed catalytic mechanism, especially for the formation of the oxyanion hole.

3.4. The inhibition of PEDV PL2^{pro}

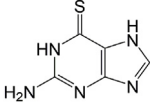
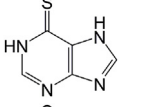
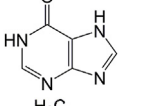
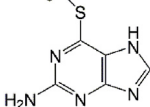
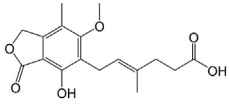
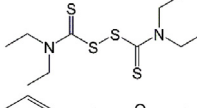
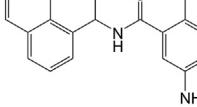
Several coronaviral PL^{pro} inhibitors have been identified in previous studies (Chen et al., 2009; Cheng et al., 2015; Chou et al., 2008; Lin et al., 2018; Ratia et al., 2008). In the present study, these compounds were screened to determine whether they can inhibit PEDV PL2^{pro} (Table 2). Among the compounds, two thiopurine analogs, 6-mercaptopurine (6MP) and 6TG, were found to be able to inhibit the DUB activity of PEDV PL2^{pro} with IC_{50} of 58.1 and 13.7 μ M, respectively (Fig. 2 and Table 2). IC_{50} of 6TG is 4.2-fold lower than that of 6MP, suggesting that the amino group of 6TG may play the role of an active pharmacophore in the inhibition. In addition, two 6MP/6TG analogs, hypoxanthine, and 2-amino-6-methyl-mercaptopurine, were also used for structure-function relationship studies. We found that replacement of the thiocarbonyl group of 6MP/6TG with either a hydroxyl or a methylthio group resulted in compounds devoid of inhibitory activity, suggesting its importance in the inhibition (Table 2).

Due to its higher inhibition capability, 6TG was chosen for further investigation. Kinetic assays at various concentrations of peptidyl substrates and 6TG were carried out to further investigate the inhibition mechanism (Fig. S6). Interestingly, the observed kinetic parameters showed a decrease in the apparent k_{cat} at increasing 6TG concentrations, whereas the apparent K_m was not affected significantly. This is clearly indicative of a noncompetitive pattern of inhibition. Indeed, the data was found to best fit to a noncompetitive inhibition model with the K_{is} of 21.1 μ M (Fig. 3 and Table 2). This result suggests that 6TG and the peptidyl substrate may bind to different sites. For comparison, 6TG shows a competitive inhibitory effect against SARS- and MERS-CoV PL^{pro}s (Cheng et al., 2015; Chou et al., 2008) but shows a noncompetitive inhibitory effect against human USP2 (Chuang et al., 2018), albeit their K_{is} are close. These results indicate that 6TG can be a broad spectrum inhibitor against human and viral DUB enzymes via different mechanisms.

3.5. Molecular docking to find the putative binding site

As 6TG is a noncompetitive inhibitor of PEDV PL2^{pro}, recognition of the binding site of 6TG will allow us to understand its inhibitory mechanism more clearly. As no detailed structural information was

Table 2
Inhibition of PEDV PL2^{PRO} by various compounds.

Name	Structure	IC ₅₀ (μM) ^a	K _{is} (μM) ^b
6TG		13.7 ± 1.7	21.1 ± 1.1
6MP		58.1 ± 5.7	–
Hypoxanthine		ND ^c	–
2-amino-6-methyl-mercaptapurine		ND ^c	–
Mycophenolic acid		> 200	–
Disulfiram		> 100	–
GRL0617		> 100	–

^a The DUB activity assay was used for the measurement of IC₅₀ (Eq. (1)).

^b Proteolytic activity at various concentrations of SARS-CoV-derived peptidyl substrate and 6TG was measured (Fig. S6 and Fig. 3) and the apparent K_{is} was determined from the best global fit of the data to a noncompetitive inhibition model (Eq. (2)). R_{sqr} was 0.964.

^c ND: IC₅₀ was not determined due to lack of inhibition at a compound concentration of 200 μM.

available, we generated a structural model of PEDV PL2^{PRO} and tried to discover a putative binding site of 6TG using *in silico* docking. Interestingly but not surprisingly, we found that the putative binding site of 6TG with the highest affinity score is near the active site and on the left side of the blocking loop (residues 196 to 202), while the ubiquitin C-terminal tail is located on the right side (Fig. 4A). In our model, 6TG has polar interactions with residues Asp195, Gly197 (on the blocking loop), Val230 and Thr231 and shows hydrophobic contact with Lys175 and Pro229. Binding of 6TG at this site may render the blocking loop less flexible and therefore disfavor catalysis. A series of noncovalent inhibitors such as compound GRL0617 shows a similar blocking effect, although they are competitive inhibitors and bind to the S3-S4 subsite (Ratia et al., 2008). For comparison, besides residue Val230, the alignment shows no sequence identity for the putative binding residues (Fig. S1, red ovals). Furthermore, the same region is occupied by residue Pro300 of SARS-CoV PL^{PRO} and residue Lys306 of MERS-CoV PL^{PRO} (Fig. 4B), indicating that this binding site may only exist in PEDV PL2^{PRO}. In contrast, previous studies suggested that the binding site of 6TG for SARS- and MERS-CoV PL^{PRO}s may be near the catalytic triad's cysteine residue due to its competitive pattern of inhibition (Cheng et al., 2015; Chou et al., 2008).

4. Conclusion

In this study, we provide a first description of the expression,

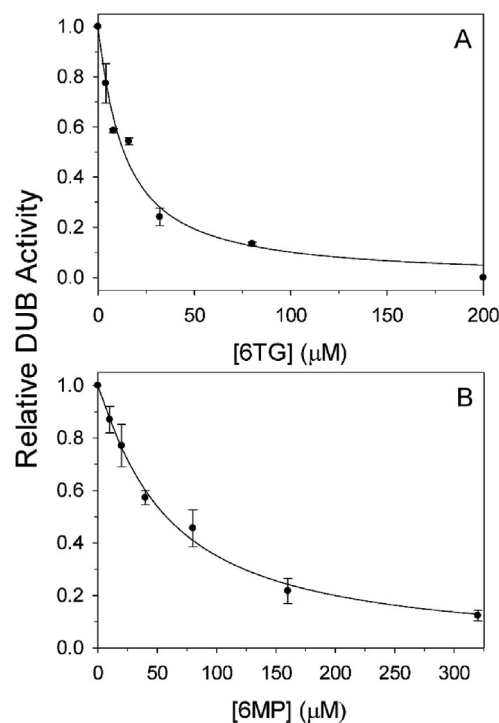


Fig. 2. Inhibitory effects of 6TG and 6MP on DUB activity of PEDV PL2^{PRO}. DUB activity of PEDV PL2^{PRO} at various concentrations of 6TG (A) or 6MP (B) was measured. The concentration of fluorogenic substrate Ub-AFC was 0.25 μM, while that of PL2^{PRO} was 0.004 μM. The lines show the best-fit results according to the IC₅₀ equation (Eq. (1)). The R_{sqr} values are 0.976 and 0.981, respectively.

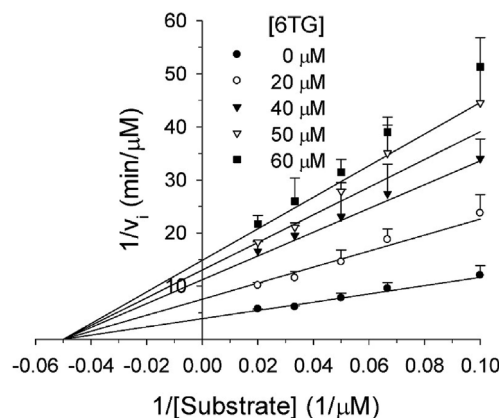


Fig. 3. Proteolytic inhibition of PEDV PL2^{PRO} by 6TG. Peptidyl substrate at concentrations of 10–50 μM and 6TG at concentrations of 0–60 μM were used for the measurements, while the protein concentration was held at 3.85 μM. The circles, squares and triangles represent mean values, while the bars represent the standard error. The solid lines show the best-fit results in accordance with a noncompetitive inhibition model (Eq. (2)) and R_{sqr} value is 0.964. The kinetic parameters from the best fit are shown in Table 1. The assay was repeated to ensure reproducibility.

purification and structural properties of PEDV PL2^{PRO} as well as its potent inhibition by thiopurine analogs. The broad spectrum inhibitor 6TG was found able to inhibit not only the DUB activity but also the proteolytic activity of PEDV PL2^{PRO}. These results shed light on the possibility of inhibition of PEDV infection by small molecules instead of antibodies. Furthermore, based on its noncompetitive inhibitory effect, we proposed an allosteric 6TG binding site which can stabilize the blocking loop near the active site, resulting in inhibition. The present study suggests that 6TG may be suitable as a lead compound for further

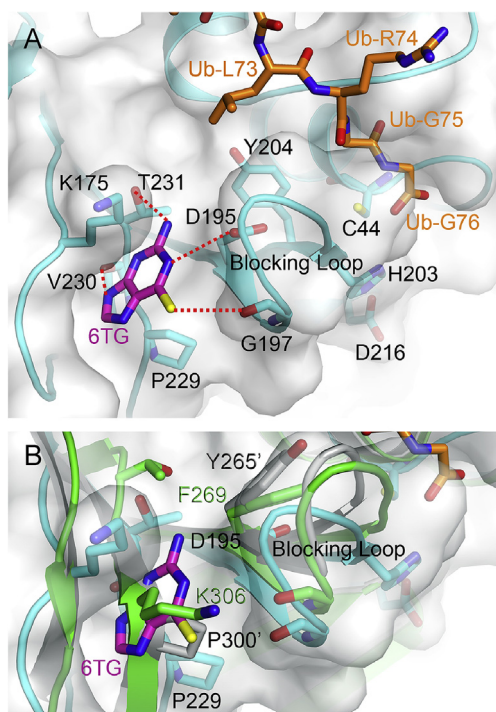


Fig. 4. Model structure of PEDV PL2^{PRO} in complex with 6TG. (A) The model structure of PEDV PL2^{PRO} (cyan) was generated by SWISS-MODEL (Arnold et al., 2006). The location of Ub (orange) is based on overlaying with the complex structure of MERS-CoV PL^{PRO} C111S – Ub (PDB code: 4WUR) (Lei and Hilgenfeld, 2016). The docking of 6TG (magenta) was performed using AutoDock Vina. The residues are shown as sticks while the putative polar interactions are shown as dotted lines. (B) Overlay of the docked model, SARS- (grey; PDB code: 4M0W) and MERS-CoV (green) PL^{PRO}-Ub complex structures. The same location is occupied by the residue Pro300 of SARS-CoV PL^{PRO} and the residue Lys306 of MERS-CoV PL^{PRO}, respectively, suggesting that 6TG cannot bind to this site in the two enzymes. The figures were produced using PyMol (<http://www.pymol.org>). (For interpretation of the references to colour in this figure legend, the reader is referred to the Web version of this article.)

antiviral drug development.

Acknowledgements

We would like to thank Prof. Ralph Kirby for helpful suggestions. We also appreciate Mrs. Yen-Su Lin's help in the synthesis of compound GRL0617. This research was supported by grants from the Ministry of Science and Technology, Taiwan, ROC (104-2320-B-010-034, 105-2320-B-010-012, 107-2320-B-010-045, and 106-2320-B-010-013) to CYC. HFC was supported by the Ministry of Education, Taiwan, R.O.C. and Bened Biomedical Co.

Appendix A. Supplementary data

Supplementary data related to this article can be found at <https://doi.org/10.1016/j.antiviral.2018.08.011>.

References

- Anand, K., Ziebuhr, J., Wadhvani, P., Mesters, J.R., Hilgenfeld, R., 2003. Coronavirus main proteinase (3CLpro) structure: basis for design of anti-SARS drugs. *Science* 300, 1763–1767.
- Arnold, K., Bordoli, L., Kopp, J., Schwede, T., 2006. The SWISS-MODEL workspace: a web-based environment for protein structure homology modelling. *Bioinformatics* 22, 195–201.
- Avvakumov, G.V., Walker, J.R., Xue, S., Finerty Jr., P.J., Mackenzie, F., Newman, E.M., Dhe-Paganon, S., 2006. Amino-terminal dimerization, NRDP1-rhodanese interaction, and inhibited catalytic domain conformation of the ubiquitin-specific protease 8 (USP8). *J. Biol. Chem.* 281, 38061–38070.
- Bacha, U., Barrila, J., Gabelli, S.B., Kiso, Y., Mario Amzel, L., Freire, E., 2008. Development of broad-spectrum halomethyl ketone inhibitors against coronavirus main protease 3CL(pro). *Chem. Biol. Drug Des.* 72, 34–49.
- Bailey-Ellkin, B.A., Knaap, R.C., Johnson, G.G., Dalebout, T.J., Ninaber, D.K., van Kasteren, P.B., Bredenbeek, P.J., Snijder, E.J., Kikkert, M., Mark, B.L., 2014. Crystal structure of the Middle East respiratory syndrome coronavirus (MERS-CoV) papain-like protease bound to ubiquitin facilitates targeted disruption of deubiquitinating activity to demonstrate its role in innate immune suppression. *J. Biol. Chem.* 289, 34667–34682.
- Bullock, A.N., Henckel, J., DeDecker, B.S., Johnson, C.M., Nikolova, P.V., Proctor, M.R., Lane, D.P., Fersht, A.R., 1997. Thermodynamic stability of wild-type and mutant p53 core domain. *Proc. Natl. Acad. Sci. U. S. A.* 94, 14338–14342.
- Chan, J.F., Lau, S.K., To, K.K., Cheng, V.C., Woo, P.C., Yuen, K.Y., 2015. Middle East respiratory syndrome coronavirus: another zoonotic betacoronavirus causing SARS-like disease. *Clin. Microbiol. Rev.* 28, 465–522.
- Chasey, D., Cartwright, S.F., 1978. Virus-like particles associated with porcine epidemic diarrhoea. *Res. Vet. Sci.* 25, 255–256.
- Chaudhuri, R., Tang, S., Zhao, G., Lu, H., Case, D.A., Johnson, M.E., 2011. Comparison of SARS and NL63 papain-like protease binding sites and binding site dynamics: inhibitor design implications. *J. Mol. Biol.* 414, 272–288.
- Chen, X., Chou, C.Y., Chang, G.G., 2009. Thiopurine analogue inhibitors of severe acute respiratory syndrome-coronavirus papain-like protease, a deubiquitinating and deISGylating enzyme. *Antivir. Chem. Chemother.* 19, 151–156.
- Cheng, K.W., Cheng, S.C., Chen, W.Y., Lin, M.H., Chuang, S.J., Cheng, I.H., Sun, C.Y., Chou, C.Y., 2015. Thiopurine analogs and mycophenolic acid synergistically inhibit the papain-like protease of Middle East respiratory syndrome coronavirus. *Antivir. Res.* 115, 9–16.
- Chou, C.Y., Chien, C.H., Han, Y.S., Prebanda, M.T., Hsieh, H.P., Turk, B., Chang, G.G., Chen, X., 2008. Thiopurine analogues inhibit papain-like protease of severe acute respiratory syndrome coronavirus. *Biochem. Pharmacol.* 75, 1601–1609.
- Chou, C.Y., Lai, H.Y., Chen, H.Y., Cheng, S.C., Cheng, K.W., Chou, Y.W., 2014. Structural basis for catalysis and ubiquitin recognition by the severe acute respiratory syndrome coronavirus papain-like protease. *Acta Crystallogr. D Biol. Crystallogr.* 70, 572–581.
- Chou, Y.W., Cheng, S.C., Lai, H.Y., Chou, C.Y., 2012. Differential domain structure stability of the severe acute respiratory syndrome coronavirus papain-like protease. *Arch. Biochem. Biophys.* 520, 74–80.
- Chuang, S.J., Cheng, S.C., Tang, H.C., Sun, C.Y., Chou, C.Y., 2018. 6-Thioguanine is a noncompetitive and slow binding inhibitor of human deubiquitinating protease USP2. *Sci. Rep.* 8, 3102.
- Clasman, J.R., Baez-Santos, Y.M., Mettelman, R.C., O'Brien, A., Baker, S.C., Mesecar, A.D., 2017. X-ray structure and enzymatic activity profile of a core papain-like protease of MERS coronavirus with utility for structure-based drug design. *Sci. Rep.* 7, 40292.
- Clementz, M.A., Chen, Z., Banach, B.S., Wang, Y., Sun, L., Ratia, K., Baez-Santos, Y.M., Wang, J., Takayama, J., Ghosh, A.K., Li, K., Mesecar, A.D., Baker, S.C., 2010. Deubiquitinating and interferon antagonism activities of coronavirus papain-like proteases. *J. Virol.* 84, 4619–4629.
- Han, Y.S., Chang, G.G., Juo, C.G., Lee, H.J., Yeh, S.H., Hsu, J.T., Chen, X., 2005. Papain-like protease 2 (PLP2) from severe acute respiratory syndrome coronavirus (SARS-CoV): expression, purification, characterization, and inhibition. *Biochemistry* 44, 10349–10359.
- Ho, B.L., Cheng, S.C., Shi, L., Wang, T.Y., Ho, K.I., Chou, C.Y., 2015. Critical assessment of the important residues involved in the dimerization and catalysis of MERS coronavirus main protease. *PLoS One* 10, e0144865.
- Huang, Y.W., Dickerman, A.W., Pineyro, P., Li, L., Fang, L., Kiehne, R., Opriessnig, T., Meng, X.J., 2013. Origin, evolution, and genotyping of emergent porcine epidemic diarrhoea virus strains in the United States. *MBio* 4, e00737-00713.
- Kumar, V., Shin, J.S., Shie, J.J., Ku, K.B., Kim, C., Go, Y.Y., Huang, K.F., Kim, M., Liang, P.H., 2017. Identification and evaluation of potent Middle East respiratory syndrome coronavirus (MERS-CoV) 3CL(Pro) inhibitors. *Antivir. Res.* 141, 101–106.
- Lee, C., 2015. Porcine epidemic diarrhoea virus: an emerging and re-emerging epizootic swine virus. *Virol. J.* 12, 193.
- Lee, C.D., Sun, H.C., Hu, S.M., Chiu, C.F., Homhuan, A., Liang, S.M., Leng, C.H., Wang, T.F., 2008. An improved SUMO fusion protein system for effective production of native proteins. *Protein Sci.* 17, 1241–1248.
- Lei, J., Hilgenfeld, R., 2016. Structural and mutational analysis of the interaction between the Middle-East respiratory syndrome coronavirus (MERS-CoV) papain-like protease and human ubiquitin. *Virol. Sin.* 31, 288–299.
- Lei, J., Kusov, Y., Hilgenfeld, R., 2018. Nsp3 of coronaviruses: structures and functions of a large multi-domain protein. *Antivir. Res.* 149, 58–74.
- Lei, J., Mesters, J.R., Drosten, C., Anemuller, S., Ma, Q., Hilgenfeld, R., 2014. Crystal structure of the papain-like protease of MERS coronavirus reveals unusual, potentially druggable active-site features. *Antivir. Res.* 109, 72–82.
- Li, C., Li, W., Lucio de Esesarte, E., Guo, H., van den Elzen, P., Aarts, E., van den Born, E., Rottier, P.J.M., Bosch, B.J., 2017. Cell attachment domains of the porcine epidemic diarrhoea virus spike protein are key targets of neutralizing antibodies. *J. Virol.* 91.
- Li, F., Li, W., Farzan, M., Harrison, S.C., 2005. Structure of SARS coronavirus spike receptor-binding domain complexed with receptor. *Science* 309, 1864–1868.
- Lin, M.H., Chuang, S.J., Chen, C.C., Cheng, S.C., Cheng, K.W., Lin, C.H., Sun, C.Y., Chou, C.Y., 2014. Structural and functional characterization of MERS coronavirus papain-like protease. *J. Biomed. Sci.* 21, 54.
- Lin, M.H., Moses, D.C., Hsieh, C.H., Cheng, S.C., Chen, Y.H., Sun, C.Y., Chou, C.Y., 2018. Disulfiram can inhibit MERS and SARS coronavirus papain-like proteases via different modes. *Antivir. Res.* 150, 155–163.
- Mielech, A.M., Kilianski, A., Baez-Santos, Y.M., Mesecar, A.D., Baker, S.C., 2014. MERS-CoV papain-like protease has deISGylating and deubiquitinating activities. *Virology* 450–451, 64–70.

- Park, J.Y., Jeong, H.J., Kim, J.H., Kim, Y.M., Park, S.J., Kim, D., Park, K.H., Lee, W.S., Ryu, Y.B., 2012. Diarylheptanoids from *Alnus japonica* inhibit papain-like protease of severe acute respiratory syndrome coronavirus. *Biol. Pharm. Bull.* 35, 2036–2042.
- Ratia, K., Pegan, S., Takayama, J., Sleeman, K., Coughlin, M., Baliji, S., Chaudhuri, R., Fu, W., Prabhakar, B.S., Johnson, M.E., Baker, S.C., Ghosh, A.K., Mesecar, A.D., 2008. A noncovalent class of papain-like protease/deubiquitinase inhibitors blocks SARS virus replication. *Proc. Natl. Acad. Sci. U. S. A.* 105, 16119–16124.
- Ratia, K., Saikatendu, K.S., Santarsiero, B.D., Barretto, N., Baker, S.C., Stevens, R.C., Mesecar, A.D., 2006. Severe acute respiratory syndrome coronavirus papain-like protease: structure of a viral deubiquitinating enzyme. *Proc. Natl. Acad. Sci. U. S. A.* 103, 5717–5722.
- Renatus, M., Parrado, S.G., D'Arcy, A., Eidhoff, U., Gerhartz, B., Hassiepen, U., Pierrat, B., Riedl, R., Vinzenz, D., Worpenberg, S., Kroemer, M., 2006. Structural basis of ubiquitin recognition by the deubiquitinating protease USP2. *Structure* 14, 1293–1302.
- Schuck, P., 2000. Size-distribution analysis of macromolecules by sedimentation velocity ultracentrifugation and lamm equation modeling. *Biophys. J.* 78, 1606–1619.
- Song, D., Moon, H., Kang, B., 2015. Porcine epidemic diarrhea: a review of current epidemiology and available vaccines. *Clin. Exp. Vaccine Res.* 4, 166–176.
- Song, D., Park, B., 2012. Porcine epidemic diarrhoea virus: a comprehensive review of molecular epidemiology, diagnosis, and vaccines. *Virus Genes* 44, 167–175.
- Stevenson, G.W., Hoang, H., Schwartz, K.J., Burrough, E.R., Sun, D., Madson, D., Cooper, V.L., Pillatzki, A., Gauger, P., Schmitt, B.J., Koster, L.G., Killian, M.L., Yoon, K.J., 2013. Emergence of Porcine epidemic diarrhea virus in the United States: clinical signs, lesions, and viral genomic sequences. *J. Vet. Diagn. Investig.* 25, 649–654.
- Trott, O., Olson, A.J., 2010. AutoDock Vina: improving the speed and accuracy of docking with a new scoring function, efficient optimization, and multithreading. *J. Comput. Chem.* 31, 455–461.
- Wang, N., Shi, X., Jiang, L., Zhang, S., Wang, D., Tong, P., Guo, D., Fu, L., Cui, Y., Liu, X., Arledge, K.C., Chen, Y.H., Zhang, L., Wang, X., 2013. Structure of MERS-CoV spike receptor-binding domain complexed with human receptor DPP4. *Cell Res.* 23, 986–993.
- Whitmore, L., Wallace, B.A., 2008. Protein secondary structure analyses from circular dichroism spectroscopy: methods and reference databases. *Biopolymers* 89, 392–400.
- Wojdyla, J.A., Manolaridis, I., van Kasteren, P.B., Kikkert, M., Snijder, E.J., Gorbelenya, A.E., Tucker, P.A., 2010. Papain-like protease 1 from transmissible gastroenteritis virus: crystal structure and enzymatic activity toward viral and cellular substrates. *J. Virol.* 84, 10063–10073.
- Wu, C.Y., King, K.Y., Kuo, C.J., Fang, J.M., Wu, Y.T., Ho, M.Y., Liao, C.L., Shie, J.J., Liang, P.H., Wong, C.H., 2006. Stable benzotriazole esters as mechanism-based inactivators of the severe acute respiratory syndrome 3CL protease. *Chem. Biol.* 13, 261–268.
- Wu, K., Li, W., Peng, G., Li, F., 2009. Crystal structure of NL63 respiratory coronavirus receptor-binding domain complexed with its human receptor. *Proc. Natl. Acad. Sci. U. S. A.* 106, 19970–19974.
- Xing, Y., Chen, J., Tu, J., Zhang, B., Chen, X., Shi, H., Baker, S.C., Feng, L., Chen, Z., 2013. The papain-like protease of porcine epidemic diarrhea virus negatively regulates type I interferon pathway by acting as a viral deubiquitinase. *J. Gen. Virol.* 94, 1554–1567.
- Yang, H., Yang, M., Ding, Y., Liu, Y., Lou, Z., Zhou, Z., Sun, L., Mo, L., Ye, S., Pang, H., Gao, G.F., Anand, K., Bartlam, M., Hilgenfeld, R., Rao, Z., 2003. The crystal structures of severe acute respiratory syndrome virus main protease and its complex with an inhibitor. *Proc. Natl. Acad. Sci. U. S. A.* 100, 13190–13195.
- Zheng, D., Chen, G., Guo, B., Cheng, G., Tang, H., 2008. PLP2, a potent deubiquitinase from murine hepatitis virus, strongly inhibits cellular type I interferon production. *Cell Res.* 18, 1105–1113.